Available online at www.sciencedirect.com

ScienceDirect

Ceramics International 40 (2014) 57–65

CERAMICS INTERNATIONAL

www.elsevier.com/locate/ceramint

Photocatalytic degradation properties of $Ni(OH)_2$ nanosheets/ZnO nanorods composites for azo dyes under visible-light irradiation

Xiaoyan Cai[a], Yun Cai[a], Yongjun Liu[b], Shaojuan Deng[a], Yan Wang[a], Yude Wang[a,c,*], Igor Djerdj[d]

[a]Department of Materials Science and Engineering, Yunnan University, 650091 Kunming, People's Republic of China
[b]Advanced Analysis and Measurement Center, Yunnan University, 650091 Kunming, People's Republic of China
[c]State Key Lab of Silicon Materials, Zhejiang University, Hangzhou 310027, People's Republic of China
[d]Ruđer Bošković Institute, Bijenička 54, 10000 Zagreb, Croatia

Received 14 April 2013; received in revised form 21 May 2013; accepted 27 May 2013
Available online 6 June 2013

Abstract

A new visible-light sensitive photocatalyst, $Ni(OH)_2$ nanosheets/ZnO nanorods composites with different $Ni(OH)_2$ contents, was synthesized via a facile water bath route. X-ray diffraction (XRD), transmission electron microscopy (TEM) and UV–vis spectroscopy were used to examine the morphology and microstructure of the composites. XRD analysis revealed that the two phases were composed of well crystallized ZnO and poorly crystallized $Ni(OH)_2 \cdot 0.75H_2O$. $Ni(OH)_2$/ZnO composites showed a red shift in band edge absorption peak in the UV–vis absorbance spectrum, which enhanced their photocatalytic activity. The composites were used for the photodecolourization of water solution of representative organic azo dyes (rhodamine B (RB), Congo red (CR), methylene blue (MB) and methyl orange (MO)) under visible light. All synthesized composites showed better photodegradation performance compared to either pure ZnO or $Ni(OH)_2$. It was noted that composites removal rate strongly depended on the $Ni(OH)_2$ content. When $Ni(OH)_2$ fraction was 10 wt% composites exhibited maximum photodegradation performance for all organic azo dyes. Finally, the possible formation mechanism of the $Ni(OH)_2$/ZnO composites and their photocatalytic decomposition mechanism were also proposed and discussed.

Keywords: Azo dyes; Nanocomposite; $Ni(OH)_2$; Photocatalysis; ZnO

1. Introduction

Large quantities of dyes used in the textile industry are lost to the effluents during manufacturing and processing operations [1]. These colored dye effluents, which are not readily biodegradable, create series of environmental pollution problems by releasing toxic and potential carcinogenic substances into the aqueous systems. Adsorption and chemical coagulation are two typical techniques of wastewater treatment. However, these methods merely transfer dye from the liquid to the solid phase causing secondary pollution and requiring further post-treatment [2]. Recent developments of advanced oxidation processes (AOPs), have led to new improvements of the oxidative destruction of dyes and many other organics in wastewater and effluents. These processes generally involve UV/H_2O_2, UV/O_3 or UV/Fenton's reagent for the oxidative degradation of contaminants, yielding encouraging results of color removal from azo-reactive dye containing waters [3]. Semiconductor photocatalysts based on AOPs were thoroughly investigated due to their high efficiency, commercial availability and high chemical stability. When the semiconductor particles are illuminated with UV-light, valence band electrons are promoted to the conduction band due to photoexcitation, leaving an electron deficiency or hole behind. Such generated electron–hole pairs can either recombine or interact separately with other molecules. Both reductive and oxidative processes can occur at or near the surface of the photoexcited semiconductor particle [4,5].

Among various semiconductor photocatalysts, TiO_2 is the most commonly used effective photocatalyst for a wide range of

*Corresponding author at: Department of Materials Science and Engineering, Yunnan University, 650091 Kunming, People's Republic of China
Tel.: +86 871 6998372.
E-mail address: ydwang@ynu.edu.cn (Y. Wang).

0272-8842/$ - see front matter © 2013 Elsevier Ltd and Techna Group S.r.l. All rights reserved.
http://dx.doi.org/10.1016/j.ceramint.2013.05.103

organic chemical degradation. However, current research reports show that ZnO can be also used as a very efficient semiconductor photocatalyst comparable to TiO_2 [6,7]. ZnO and TiO_2 have similar bandgaps around 3.2 eV [8,9].The quantum efficiency of ZnO powder is also significantly larger than that of TiO_2 powder, and higher catalytic efficiencies of some azo-reactive dyes in aqueous solutions have been reported for ZnO [10–12].

Unfortunately, the photocatalytic efficiency on a bare ZnO is very low, mainly due to the rapid recombination of photogenerated electrons and holes. On the other hand, because of the large band gap (3.2 eV) all photon-driven applications of ZnO require ultraviolet light ($\lambda < 387$ nm) for excitation [13]. To overcome these shortcomings and enhance photocatalytic activity of ZnO to the visible region, many efforts have been made, including noble metal modifying [14], non-metallic elements doping (e.g. C, N, S) [15–17], rare-earth ion doping (e.g. Ce, La) [18,19] and transitional metal doping (e.g. Ni, Mn, Co, Fe, Cu) [20–24]. Moreover, some mixed oxide semiconductors composed of two or more oxide particles with different energy levels exhibit better photocatalytic activity due to more efficient charge separation. The previous work showed that NiO–ZnO composite was a cost-effective and efficient photocatalyst. For example, Zhang et al. [25] and Hameed et al. [26] reported that the NiO–ZnO nanocomposites synthesized through electrospinning technique and co-precipitation/co-gel formation technique, respectively, exhibited better photocatalytic activity than pure ZnO and NiO in the degradation of organic dyes under the irradiation of UV-light, and both of them attributed the results to the formation of p–n heterojunctions in the NiO–ZnO nanocomposites. In addition, Yu et al. [27] investigated the fabrication of $Ni(OH)_2$ modified TiO_2 ($Ni(OH)_2/TiO_2$) nanocomposite and its photocatalytic activity for water splitting to produce H_2 under UV irradiation. However, to our best knowledge, there is no report on the visible-light photocatalytic decomposition of azo-reactive dyes using $Ni(OH)_2$/ZnO composites.

In this paper, we report a simple water bath method for the fabrication of the $Ni(OH)_2$ nanosheets/ZnO nanorods composite photocatalysts and their enhanced photocatalystic degradation activity for some azo dyes: rhodamine B, Congo red, methylene blue and methyl orange under the visible light. The structure, morphology and composition of the as-synthesized samples were characterized by X-ray diffraction analysis (XRD) and transmission electron microscopy (TEM). UV–vis spectroscopy was taken to explore their optical properties. Also a mechanism for photocatalytic decomposition in Ni$(OH)_2$/ZnO was proposed.

2. Experimental details

2.1. Synthesis of $Ni(OH)_2$ nanosheets-ZnO nanorods composites

All the chemical reagents used in the experiments were obtained from commercial sources as guaranteed-grade reagents and used without further purification.

In a typical experiment, 1.7 g zinc chloride ($ZnCl_2$) was mixed with distilled deionized water (20 mL) under vigorous stirring until a homogenous solution was obtained. The various quantitites of nickel chloride hexahydrate ($NiCl_2 \cdot 6H_2O$) solution (5 mL) were added into the $ZnCl_2$ solution in order to achieve a sequence of Ni^{2+}/Zn^{2+} molar ratios: 0.3, 0.5, 0.8, 1.0 and 2.0. After stirring for 10 min, appropriate amount of the mixing solution was dribbled into 5 M NaOH solution (20 mL) with an OH^-/Zn^{2+} molar ratio of 10. Then, 35 mL of the reaction mixture was transferred into a flask filled with distilled deionized water (20 mL), and the flask was kept at 90 °C for 24 h under a water bath condition. Finally, the powder products were obtained through centrifugation, washing, drying and collection. The as-prepared samples in subsequent discussions of this paper were designated as 0.3NZ, 0.5NZ, 0.8NZ, 1.0NZ and 2.0NZ, respectively. The synthesis procedure for the pure ZnO and $Ni(OH)_2$ was the same as above mentioned.

2.2. Characterization

Powder X-ray diffraction (XRD) data were carried out with a Rigaku D/MAX-3B powder diffractometer using Cu$K\alpha$ radiation ($\lambda = 1.54056$ Å). The samples were scanned from 5° to 90° (2θ) in steps of 0.02°. Transmission electron microscopy (TEM) measurement was performed on a Zeiss EM 912 Ω instrument at an acceleration voltage of 120 kV. The samples for TEM were prepared by dispersing the final samples in distilled deionized water; this dispersion was then dropped on carbon–copper grids coated by an amorphous carbon film. To prevent agglomeration of nanostructures, the copper grid was placed on a filter paper at the bottom of a Petri dish. UV/vis measurements were made with a Hitachi U-4100 spectrophotometer with a wavelength range between 200 and 800 nm.

2.3. Measurement of degradation properties for azo dyes

The photodecolourization of azo dyes in aqueous solution was studied in the presence of as-synthesized $Ni(OH)_2$/ZnO nanocomposite powders. The dye aqueous solutions of RB, CR, MB and MO were prepared by dissolving analytical grade dye in water. Ten milligrams of the photocatalyst powders were added into 50 mL of RB, CR, MB and MO aqueous solutions with a concentration of 1×10^{-5} M in a quartz beaker, respectively. The reaction mixtures were irradiated by a visible-light lamp with a filter to cut the UV region and magnetically stirred throughout the photocatalytic experiment under air at room temperature. The distance between the visible-light lamp and the solution surface was 8 cm. The average intensity of visible-light reaching the surface of solutions was measured to be ca. 0.8 mW/cm^2. The reactors were sealed to prevent any evaporation of the solutions. During irradiation, and four milliliter of the dispersion was continually extracted at given time and subsequently centrifuged to separate catalyst and dye solutions at 4000 rev min^{-1} for 30 min. For comparison of the effect of photolysis and adsorption on the degradation properties, measured without

any photocatalyst powders under visible light (photolysis experiments) and in the dark with photocatalyst powders (adsorption experiments), for RB, CR, MB and MO aqueous solutions with a concentration of 1×10^{-5} M in a quartz beaker were carried out. The concentration (C) of the centrifuged solution and the initial concentration (C_o) of RB, CR, MB and MO solution were monitored immediately by measuring the absorbance of the different supernatant at maximum absorption wavelength of 550, 498, 664 and 463 nm, respectively, using the absorbance model by a spectrophotometer (model no. JH722N).

3. Results and discussion

3.1. Structure, morphology and component

The representative XRD patterns of as prepared composites denoted as 0.5NZ, 1.0NZ, pure ZnO and pure $Ni(OH)_2$ are presented in Fig. 1. All diffraction peaks in Fig. 1(c) and (g) can be perfectly indexed to the hexagonal wurtzite structure of ZnO (Zinc Oxide, JCPDS card no. 36-1451) or hexagonal crystal structure of $Ni(OH)_2$ (Nickel Hydroxide, JCPDS card no. 73-1520), respectively. The diffraction peaks are sharp and intense for the pure ZnO, but broad and relatively weak for Ni $(OH)_2$, suggesting the different crystalline character of the pure phases prepared under similar water bath condition. Hence, ZnO is more easily crystallized at low temperature (90 °C). As observed in Fig. 1(d) and (e), two sets of diffraction peaks exist for the sample 0.5NZ and 0.1NZ, which are correspondingly assigned to the hexagonal structure ZnO and hexagonal structure $Ni(OH)_2 \cdot 0.75H_2O$ (nickel hydroxide hydrate, JCPDS card no. 38-0715). No characteristic peaks for byproducts, such as $ZnCl_2$, $NiCl_2$ or other zinc nickel oxides, are found in the patterns, indicating the formation of $Ni(OH)_2$/ZnO composites.

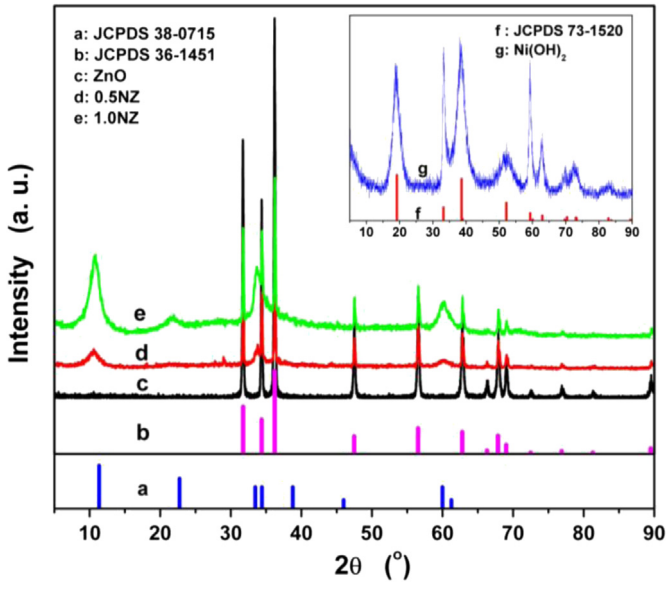

Fig. 1. XRD patterns of as-synthesized pure ZnO, pure $Ni(OH)_2$, and $Ni(OH)_2$ nanosheets/ZnO nanorods composite.

Further observation from Fig. 1 shows that there is no shift of the ZnO diffraction peaks, suggesting that the deposited Ni $(OH)_2 \cdot 0.75H_2O$ clusters do not incorporate into the lattice of ZnO [28]. Nonetheless, by comparison of $Ni(OH)_2 \cdot 0.75H_2O$ diffraction peaks intensities for various samples, it appears that its intensities are gradually increased upon increasing the molar ratio of Ni to Zn from 0 to 0.5 and 1 (from pure ZnO to 0.5NZ and 1.0NZ). Besides, it is worth noting that the products are nickel hydroxide hydrate instead of pure nickel hydroxide when forming a complex with zinc oxide, symptomatic of an interaction between the components of the composites. This interaction will be discussed below in the section of the growth mechanism.

TEM investigations provide insight into the morphological and structural features of the $Ni(OH)_2$/ZnO nanostructured composites. Fig. 2 shows the representative low-magnification TEM and high-resolution transmission electron microscopy (HRTEM) images of pure ZnO, $Ni(OH)_2$ and 1.0NZ. From Fig. 2(a), although there some short ZnO nanorods which adhering impurities on the surface, it is clearly visible that most of the pure ZnO nanorods are cone-shaped in morphology and smooth at surface. The average diameter of pure ZnO nanorods is around 500 nm and the length is up to 1–5 μm. The pure $Ni(OH)_2$ nanostructures synthesized by the same process as shown in Fig. 2(c) display the uniform morphology of flake-like nanostructures with typical length in the range of several to several tens of nanometers. The image also demonstrates that the $Ni(OH)_2$ nanosheets are very thin. Fig. 2(b) and (d) depict that the space between two adjacent lattice planes is 0.26 and 0.24 nm, respectively, which correspond to (0 0 2) planes of hexagonal ZnO and (0 1 1) planes of hexagonal $Ni(OH)_2$. Fig. 2(e) exhibits a low magnification TEM image of the sample 1.0NZ. As it can be seen from this image, a layer of $Ni(OH)_2 \cdot 0.75H_2O$ with a thickness in the range of several tens to several hundreds of nanometers is deposited on the surface of the ZnO nanorods. It also reveals the simultaneous presence of the adhering and individual nickel hydroxide hydrate clusters, indicating that not all $Ni(OH)_2 \cdot 0.75H_2O$ is intimately deposited on the surface of ZnO nanorods. HRTEM images of ZnO and Ni $(OH)_2 \cdot 0.75H_2O$ compounds which constitute the sample 1.0NZ are shown in Fig. 2(f) and (g), respectively. The depicted nanorod with a calculated d-spacing of 0.27 nm correspond to the (0 0 2) planes of the hexagonal ZnO. The interplanar distances of 0.31 nm are close to the lattice spacing of the (0 0 1) planes of the hexagonal $Ni(OH)_2 \cdot 0.75H_2O$. Moreover, a more detailed observation indicates that the surface of nanorods appear to be modified due to the occurrence of nickel hydroxide hydrate nanosheet clusters. Most transition metal ions are known to remain preferably in aqueous solution as stable complexes, not to incorporate into zinc site, and the formation of secondary phases related to transition metal ions or variation can result in the change of morphology [29,30]. XRD study showed that $Ni(OH)_2 \cdot 0.75H_2O$ could suppress the nucleation and growth of ZnO, resulting in spatial distribution of Ni related nanoparticles. Although slight modification in the surface of the rods is observed with the

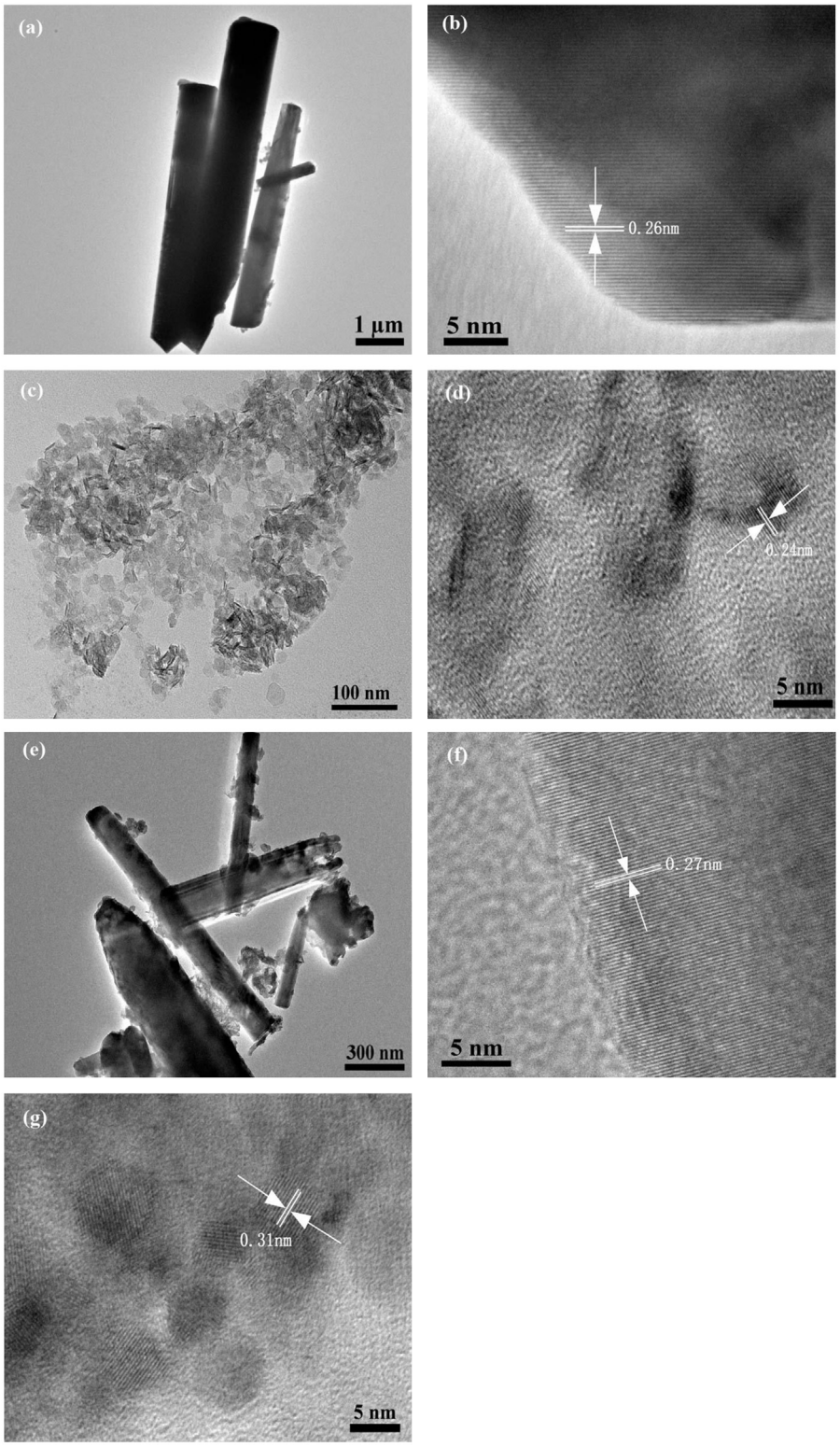

Fig. 2. TEM images of pure ZnO, pure $Ni(OH)_2$, and $Ni(OH)_2$/ZnO composite at low magnification and at high magnification: (a) and (b) ZnO; (c) and (d) Ni $(OH)_2$; (e)–(g) 1.0NZ.

coupling of composites, overall anisotropic growth of ZnO is maintained.

The optical properties of photocatalytic materials are of ultra most importance because they dictate the number of photons absorbed by the system. UV–vis spectroscopy is performed on the as-fabricated photocatalysts to observe changes in optical properties as a function of material composition. The UV–vis absorption spectra of $Ni(OH)_2$/ZnO composites with various

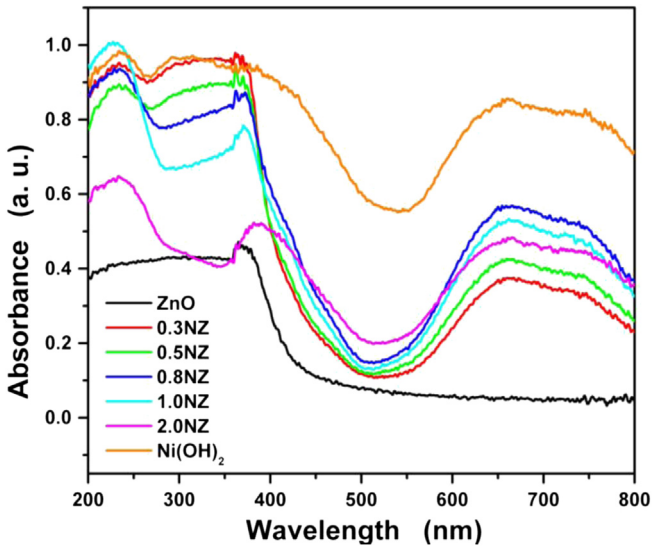

Fig. 3. UV–vis absorption spectra of pure ZnO, pure $Ni(OH)_2$, and $Ni(OH)_2$/ZnO composites.

molar ratio of Ni to Zn are presented in Fig. 3. It is found that while pure ZnO has no absorption in the visible region (400–800 nm), pure $Ni(OH)_2$ show very broad absorption bands spanning the visible region. As for sample 0.3NZ, 0.5NZ, 0.8NZ, 1.0NZ and 2.0NZ, except the strong absorption band at ultraviolet region which coincide with the intrinsic absorption of ZnO, the spectra also show absorption in the 600–800 nm region, in addition to the onset of absorption at about 450 nm [31]. According to the viewpoint of Irie et al. [32], the 600–800 nm absorption can be assigned to the Ni(II) d–d transition, and the absorption at 450 nm of $Ni(OH)_2$/ZnO can be ascribed to the direct interfacial charge transfer (IFCT) from the VB of ZnO to Ni(II). Therefore, it can be seen that the absorption at 450 and 600–800 nm increases with fraction of the deposited $Ni(OH)_2$. These results suggest that the prepared $Ni(OH)_2$/ZnO nanostructures have potential capacities of photocatalytic activity utilizing sunlight. Concerning the ZnO bulk absorption edge appearing at 373 nm at room temperature [33,34], it was found a red-shift of 68–81 nm in the band-edge for all samples by the UV–vis spectroscopy. This indicates that the optical band gap of the $Ni(OH)_2$/ZnO composites prepared by a water bath method emerges a decrease with the coupling of nanorods and nanosheets. However, in comparison to pure ZnO, no great change in the absorption edge of the $Ni(OH)_2$/ZnO samples are observed, implying that $Ni(OH)_2$ is not incorporated into the lattice of ZnO, only deposited on its surface. This result is not surprising because low-temperature deposition of $Ni(OH)_2$ does not have enough energy for Ni^{2+} to enter the lattice of ZnO [27].

On the basis of the above analysis, the probable formation mechanism of the $Ni(OH)_2$ nanosheets/ZnO nanorods composites has been proposed. At the stage of the precursor solution preparation, the finally obtained solution was clear and transparent without any generated precipitation or suspensions for pure ZnO, while for pure $Ni(OH)_2$ as well as $Ni(OH)_2$/ZnO, the solution was green and turbid. Therefore, the reaction process at this stage for $Ni(OH)_2$/ZnO composites was proposed as follows:

$$Zn^{2+}+Ni^{2}+OH^{-}\leftrightarrow Ni(OH)_2/Zn(OH)_4^{2-} \quad (1)$$

At the solution configuring course, Zn^{2+} and Ni^{2+} ions were added to the alkaline solution. The aquaeous precipitate appeared at once and gradually increased by the addition of $ZnCl_2$ and $NiCl_2$ mixed solution, which demonstrated that the reaction occurred and $Ni(OH)_2$ emerged. In the meantime, the $Zn(OH)_2$ generated in this system was immediately dissolved by the excess of OH^- ions, and ultimately form an over-saturated $Zn(OH)_4^{2-}$ solution, as shown in the reaction Eq. (1). Based on the XRD results, one can see that all identified compounds ZnO and $Ni(OH)_2\cdot 0.75H_2O$, crystallized in the hexagonal system. The growth process of such crystals can be divided into two phases: nucleation and crystal growth. When heating the precursor solution, $Zn(OH)_4^{2-}$ ions, which coated with the $Ni(OH)_2$ micelles, transformed into $[Zn_xO_y(OH)_z]^{(z+2y-2x)-}$ through the dehydration and bonding reaction [35]. Simultaneously, the removed water molecules were adsorbed by $Ni(OH)_2$ micelles, giving rise to the formation of $Ni(OH)_2\cdot nH_2O$ ($n=0.75$ when it comes to this study). Once the $[Zn_xO_y(OH)_z]^{(z+2y-2x)-}$ reached a certain value, there would be a reaction formulated as follow:

$$Ni(OH)_2/Zn(OH)_4^{2-}\rightarrow Ni(OH)_2\bullet nH_2O/ZnO+OH^- \quad (2)$$

Upon prolongation of the heating-treatment time, the nuclei precipitates, and crystal further grows on the basis of nuclei aggregation. The specific procedure comprises: (a) Large amount of ZnO nuclei produced in the super-saturated solution under heating condition; (b) a mass of ZnO and $Ni(OH)_2\cdot nH_2O$ nuclei gathered though mutual effect, forming highly active sites of the body surface. The active sites caused further growth of the crystal planes with low surface activity ((0 0 2) planes for ZnO and (0 0 1) planes for $Ni(OH)_2\cdot nH_2O$); (c) this trend of growth along respective directions formed the shape of the $Ni(OH)_2$ nanosheets/ZnO nanorods composite.

3.2. Degradation properties of azo dyes

The photocatalytic performances of $Ni(OH)_2$/ZnO nanocomposite were evaluated by examining the photodegradation properties of azo dyes (RB, CR, MB and MO) under visible light illumination at wavelengths longer than 420 nm, since all of the obtained composites samples have a broad adsorption in visible light region.

RB was used as one of the test contaminants because it has been extensively used as an indicator for the photocatalytic activity owing to its absorption peaks in the vis range [25,36,37]. The results of the RB degradation in the presence of $Ni(OH)_2$ nanosheets/ZnO nanorods composite with different Ni contents are summarized in Fig. 4(a), where C_o and C are the initial concentration before reaction and the reaction concentration of RB at time t, respectively. To demonstrate the synergy-induced enhancement of the photocatalytic efficiency of $Ni(OH)_2$/ZnO nanocomposite, contrastive experiments were performed using

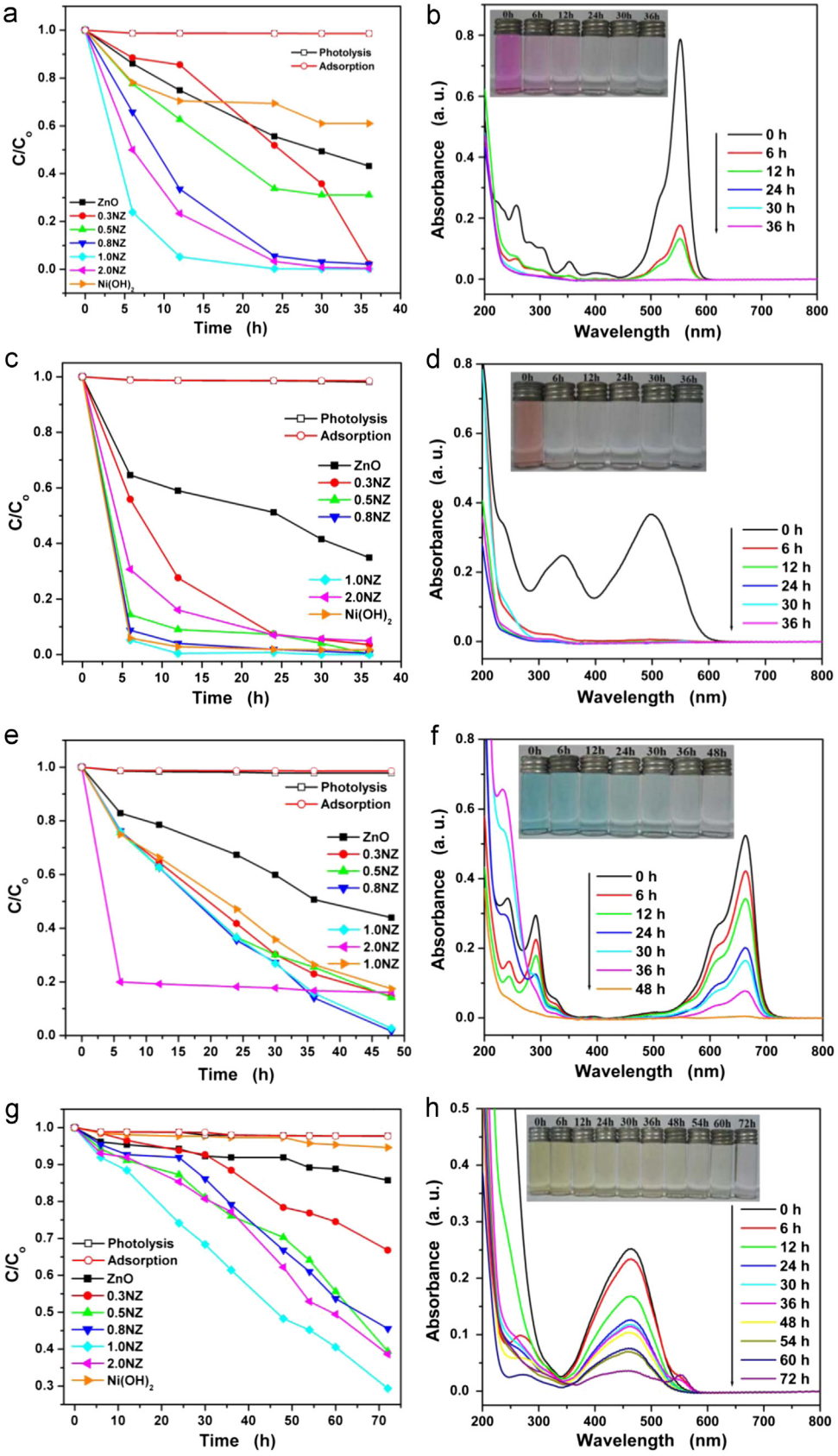

Fig. 4. Photocatalytic activity for azo dyes under visible-light irradiation in the presence of all of the as-synthesized samples at different time intervals, and UV–vis absorption spectra of azo dyes before and after treatment with sample 1.0NZ at corresponding time intervals: (a) and (b) RB; (c) and (d) CR; (e) and (f) MB; (g) and (h) MO. Photographs of the azo dye solutions during the process as inset. (For interpretation of the references to color in this figure legend, the reader is referred to the web version of this article.)

pure ZnO nanorods and $Ni(OH)_2$ nanosheets as photocatalyst for the photodegradation of RB. The reduction in the concentration of RB decreased with exposure time indicates the photocatalytic degradation of the organic dye. 1.0NZ ($Ni(OH)_2$/ZnO composite with a Ni/Zn ratio of 1.0) was found to be the most active composite, which approximately 76.1% of RB is removed under the visible light irradiation in the first 6 h, comparing to about 11.5, 22.4, 34.2 and 50.1% for samples 0.3NZ, 0.5NZ, 0.8NZ and 2.0NZ, respectively. As expected, both pure ZnO and $Ni(OH)_2$ display very poor activity that only about 56.8 and 39.2% of the dye is removed in the 36 h of exposure. Fig. 4(b) shows the variation in the UV–vis absorption spectra of the aqueous solution of RB before and after treatment with sample 1.0NZ at different time intervals. It can be seen that the maximum absorbance at 550 nm decreased rapidly with extension of the exposure time, and almost disappears after about 12 h. Further exposure leads to no absorption peak in the whole spectrum. The color change sequence in the RB solution during this process is shown in the inset of Fig. 4(b), from which it is clear that the intense rose color of the initial solution gradually disappears with increasingly longer exposure time.

CR is a sulphonated compound with two sulphonic acid groups. The absorption spectra of the CR solutions are characterized by one main band in the visible region with its maximum absorption at 498 nm corresponding to the azo bonds of the CR molecule, which is responsible for the coceine red color of aromatic rings pertaining to azo groups [38,39]. Its photocatalytic decolourization was studied in different precursors as above discussed. As depicted in Fig. 4(c), while all the $Ni(OH)_2$/ZnO composites as well as pure $Ni(OH)_2$ are able to almost fully decolorize the dye within 36 h of illumination, the pure ZnO shows significant less efficiency in the same period of time. The reason is being increase in surface defects on account of coupling of ZnO and $Ni(OH)_2$ leading to enhanced absorption in the visible region. Also the chromogen of CR can be effectually destroyed in the case of pure $Ni(OH)_2$ nanosheets existence. Compared with RB solution, higher degradation efficiency of the $Ni(OH)_2$/ZnO samples for CR solution with the same concentration can be observed. The plot of absorption versus wavelength at various times for the photodegradation of CR with sample 1.0NZ, the most active composite, is represented in Fig. 4(d), where photograph of CR solutions at the corresponding time intervals as inset. It is visible in graph that the disappearance of the adsorption band centered at 343 nm and 498 nm is accompanied by the total discoloration of the solutions in the presence of sample 1.0NZ, which degrades the practically 100% of dye within 6 h.

MB with S and N linkages in its molecular structure is a well known class of azo dye, which is cationic in aqueous media and absorbs the light in the visible region (700–550 nm) with the absorption maxima at 664 nm [26,40]. Fig. 4(e) gives the results of the photocatalytic treatment of MB using all of $Ni(OH)_2$/ZnO composites and the pure individual components. In the presence of pure ZnO nanorods, just about 56.0% of MB is removed after 48 h of irradiation. By comparison, the degradation rate of MB in the presence of $Ni(OH)_2$ nanosheets is 82.6% under the same condition. However, $Ni(OH)_2$/ZnO composites are found to exhibit more prominent photocatalytic efficiency, and as uppermost as 98.4% of MB was photodegraded from the aqueous solution after visible-light irradiation for 48 h, when it comes to sample 1.0NZ. An interesting phenomenon was observed that both the blue color of MB solution and the green color of sample powder dramatically turned into mazarine color once the 10 mg of sample 2.0NZ powder was introduced into the 50 mL of MB solution, giving rise to the constant 83.9% removal ratio of MB. This occurrence is probably due to the quick adsorption resulting from the ultra-high surface area in the abundant $Ni(OH)_2$ nanosheets and their interfaces with ZnO nanorods. From Fig. 4(f), it can be seen that in the presence of sample 1.0NZ, the amplitude of the characteristic peak decreased with respect to the treatment time and correspondingly the blue color of starting solution gradually disappears along with increasing degradation time.

MO is an azo dye characterized by N=N linkage, which is anionic in aqueous media and absorbs light in the visible region (450–550 nm) with an absorption maxima at 463 nm [26]. The photodegradation efficiencies of MO as a function of irradiation time by different as-prepared samples and the time-dependent absorption spectra of MO solution with sample 1.0NZ are shown in Fig. 4(g) and (h), respectively. It can be perceived that pure ZnO and pure $Ni(OH)_2$ have just slightly effective to MO after being irradiated under visible light for long-playing 72 h. Nevertheless, merely 70.6% of MO is photodegraded even though in the presence of the most efficient case of 1.0NZ sample in the same period of time. The tardy intensity of the main absorption bands decreases and accordingly the unconspicuous discoloration of the dye indicate that the molecular structure of MO is stable enough and difficult to be destroyed by the resultant photocatalyst as compared with those of other dyes (RB, CR and MB).

The results show that the pure ZnO and $Ni(OH)_2$ nanostructures exhibit weak visible-light photocatalytic decolourization activity for the examined azo dyes. When ZnO is coupled with $Ni(OH)_2$, the removal rate of the photocatalysts is strongly enhanced. The photodecolourization performance of $Ni(OH)_2$/ZnO composites is dependent on the proportion of Ni $(OH)_2$ in the composite. In general, the degradation rate of Ni $(OH)_2$/ZnO composites increases with the increase of $Ni(OH)_2$ content from 30 to 100 at%, but decreases when the content of $Ni(OH)_2$ exceeds 100 at%. Based on our experimental results and previous literature records, a possible photocatalytic mechanism in our experiment is proposed as shown in Fig. 5. Although the absorption edge of ZnO nanorods red shift to over 400 nm and theoretically the charges can generate and transfer between valence band (VB) and conduction band (CB) upon vis-light irradiation (see the section of UV–vis absorption analysis), the rate of azo dyes degradation is negligible over bare ZnO in the absence of $Ni(OH)_2$ nanosheets due to the rapid recombination of electrons and holes. Once $Ni(OH)_2$ is introduced to ZnO, the VB electrons of ZnO are excited to CB by visible light irradiation. Thus the photostimulated electrons in the CB of ZnO can transfer to Ni $(OH)_2$ nanosheets and then effectually reduce partial Ni^{2+} to

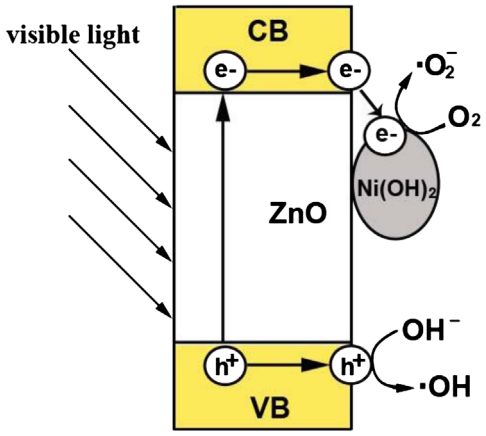

Fig. 5. Schematic illustration for photodegradation mechanism, and the charge transfer and separation in the $Ni(OH)_2$ nanosheets/ZnO nanorods composites under visible-light irradiation.

neutral Ni^0 atoms, finally forming Ni atoms or clusters [27,41,42]. As a result, these Ni atoms or clusters can act as co-catalyst to promote the separation and transfer of light-produced electrons from CB of ZnO to $Ni(OH)_2$/Ni clusters. On the other hand, a portion of separated electrons and holes can be achieved at the $Ni(OH)_2$/ZnO interfaces, which reduce their recombination probability a certain extent and enable them to migrate effectively to the surfaces of ZnO and Ni $(OH)_2$, to produce hydroxyl radicals ($OH^{\bullet}$) which are strong oxidizing agents for decomposing the organic azo dyes [43]:

$$AZO+OH^{\cdot} \rightarrow AZO_{ox}(\text{intermediates}) \rightarrow CO_2+H_2O \quad (3)$$

From Fig. 4(a), (c), (e) and (g), one can notice that the photolysis under visible light and the adsorption in the dark exhibit no degradation activity. Therefore, this comparison experiment additionally confirms the proposed degradation mechanism of azo dyes in the presence of $Ni(OH)_2$/ZnO composites as the photocatalytic degradation.

4. Conclusions

The $Ni(OH)_2$ nanosheets/ZnO nanorods composites were successfully synthesized through a simple water bath method at a low temperature. The XRD, TEM and UV–vis results confirmed that the stable and good crystalline composites composed of ZnO nanorods and $Ni(OH)_2$ nanosheets were obtained. For the photodegradation of azo dyes from water under visible-light irradiation, $Ni(OH)_2$/ZnO composites exhibited higher photocatalytic efficiency than the individual components. The improved photodecolourization performance of $Ni(OH)_2$/ZnO composites can be attributed to the reduced $Ni(OH)_2$/Ni co-catalyst, which favors the photogenerated electrons transfer from CB of ZnO to $Ni(OH)_2$. $Ni(OH)_2$/ZnO composites can be a potential candidate for applications relating to a number of environmental issues.

Acknowledgement

This work was supported by the Department of Science and Technology of Yunnan Province via the Project for the Promotion of Science and Technology (Grant No.2011FA001), National Natural Science Foundation of China (No.51262029) and the State Key Laboratory of Silicon Materials visiting scholar Fund (Grant No. SKL2012-16).

References

[1] A. Reife, H.S. Fremann, Environmental Chemistry of Dyes and Pigments, Wiley, New York307–316.
[2] K. Tanaka, K. Padermpole, T. Hisanaga, Photocatalytic degradation of commercial azo dyes, Water Research 34 (2000) 327–333.
[3] D. Georgiou, P. Melidis, A. Aivasidis, K. Gimouhopoulos, Degradation of azo-reactive dyes by ultraviolet radiation in the presence of hydrogen peroxide, Dyes and Pigments 52 (2002) 69–78.
[4] W.Z. Tang, An. Huren, UV/TiO_2 photocatalytic oxidation of commercial dyes commercial dyes in aqueous solutions, Chemosphere 31 (1995) 4157–4170.
[5] V. Augugliaro, M. Litter, L. Palmisano, J. Soria, The combination of heterogeneous photocatalysis with chemical and physical operations: a tool for improving the photoprocess performance, Journal of Photochemistry and Photobiology C: Photochemistry Reviews 7 (2006) 127–144.
[6] D. Li, H. Haneda, Morphologies of zinc oxide particles and their effects on photocatalysis, Chemosphere 51 (2003) 129–137.
[7] C. Hariharan, Photocatalytic degradation of organic contaminants in water by ZnO nanoparticles: revisited, Applied Catalysis A: General 304 (2006) 55–61.
[8] S.K. Pardeshi, A.B. Patil, Solar photocatalytic degradation of resorcinol a model endocrine disrupter in water using Zinc oxide, Journal of Hazardous Materials 163 (2009) 403–409.
[9] C. Bouvy, W. Marine, R. Sporken, B.L. Su, Photoluminescence properties and quantum size effect of ZnO nanoparticles confined inside a faujasite X zeolite matrix, Chemical Physics Letters 428 (2006) 312–316.
[10] C. Lizama, J. Freer, J. Baeza, H.D. Mansilla, Optimized photodegradation of reactive blue 19 on TiO_2 and ZnO suspensions, Catalysis Today 76 (2002) 235–246.
[11] S. Sakthivel, B. Neppolian, M.V. Shankar, B. Arabindoo, M. Palanichamy, V. Murugesan, Solar photocatalytic degradation of azo dye: comparison of photocatalytic efficiency of ZnO and TiO_2, Solar Energy Materials and Solar Cells 77 (2003) 65–82.
[12] N. Daneshvar, D. Salari, A.R. Khataee, Photocatalytic degradation of azo dye acid red 14 in water on ZnO as an alternative catalyst to TiO_2, Journal of Photochemistry and Photobiology A: Chemistry 162 (2004) 317–322.
[13] K.M. Parid, S. Parij, Photocatalytic degradation of phenol under solar radiation using microwave irradiated zinc oxide, Solar Energy 80 (2006) 1048–1054.
[14] R. Georgekutty, M.K. Seery, S.C. Pillai, A highly efficient Ag–ZnO photocatalyst: synthesis, properties, and mechanism, Journal of Physical Chemistry C 112 (2008) 13563–13570.
[15] A.B. Patil, K.R. Patil, S.K. Pardeshi, Ecofriendly synthesis and solar photocatalytic activity of S-doped ZnO, Journal of Hazardous Materials 183 (2010) 315–323.
[16] L.C. Chen, Y.J. Tu, Y.S. Wang, R.S. Kan, C.M. Huang, Characterization and photoreactivity of N-, S-, and C-doped ZnO under UV and visible light illumination, Journal of Photochemistry and Photobiology A: Chemistry 199 (2008) 170–178.
[17] S.F. Chen, W. Zhao, S.J. Zhang, W. Liu, Preparation, characterization and photocatalytic activity of N-containing ZnO powder, Journal of Chemical Engineering 148 (2009) 263–269.

[18] M. Yousefi, M. Amiri, R. Azimirad, A.Z. Moshfegh, Enhanced photoelectrochemical activity of Ce doped ZnO nanocomposite thin films under visible light, Journal of Electroanalytical Chemistry 661 (2011) 106–112.
[19] S. Anandan, A. Vinu, K.L.P. Sheeja Lovely, N. Gokulakrishnan, P. Srinivasu, T. Mori, V. Murugesan, V. Sivamurugan, K. Ariga, Photocatalytic activity of La-doped ZnO for the degradation of monocrotophos in aqueous suspension, Journal of Molecular Catalysis A: Chemical 266 (2007) 149–157.
[20] J. Zhao, L. Wang, X. Yan, Y. Yang, Y. Lei, J. Zhou, Y. Huang, Y. Gu, Y. Zhang, Structure and photocatalytic activity of Ni-doped ZnO nanorods, Materials Research Bulletin 46 (2011) 1207–1210.
[21] Q. Xiao, L. Ouyang, Photocatalytic photodegradation of xanthate over $Zn_{1-x}Mn_xO$ under visible light irradiation, Journal of Alloys and Compounds 479 (2009) 4–7.
[22] C. Xu, L. Cao, G. Su, W. Liu, X. Qu, Y. Yu, Preparation, characterization and photocatalytic activity of Co-doped ZnO powders, Journal of Alloys and Compounds 497 (2010) 373–376.
[23] Q. Xiao, C. Yao, Preparation and visible light photocatalytic activity of $Zn_{1-x}Fe_xO$ nanocrystalline, Materials Chemistry and Physics 130 (2011) 5–9.
[24] R. Mohan, K. Krishnamoorthy, Sang-Jae Kim, Enhanced photocatalytic activity of Cu-doped ZnO nanorods, Solid State Communications 152 (2012) 375380.
[25] Z. Zhang, C. Shao, X. Li, C. Wang, M. Zhang, Y. Liu, Electrospun nanofibers of p-type NiO/n-type ZnO heterojunctions with enhanced photocatalytic activity, Journal of Applied Material Interface 2 (2010) 2915–2923.
[26] A. Hameed, T. Montini, V. Gombac, P. Fornasiero, Photocatalytic decolourization of dyes on NiO–ZnO nano-composites, Journal of Photochemistry and Photobiology Science 8 (2009) 677–682.
[27] J. Yu, Y. Hai, B. Cheng, Enhanced photocatalytic H_2-production activity of TiO_2 by $Ni(OH)_2$ cluster modification, Journal of Physical Chemistry C 115 (2011) 4953–4958.
[28] C. Cheng, G. Xu, H. Zhang, Y. Luo, Hydrothermal synthesis Ni-doped ZnO nanorods with room-temperature ferromagnetism, Materials Letters 62 (2008) 1617–1620.
[29] N.S. Norberg, K.R. Kittilstved, J.E. Amonette, R.K. Kukkadapu, D. A. Schwartz, D.R. Gamelin, Synthesis of colloidal Mn^{2+}: ZnO quantum dots and high-T_C ferromagnetic nanocrystalline thin films, Journal of the American Chemical Society 126 (2004) 9387–9398.
[30] E. Liu, P. Xiao, J.S. Chen, B.C. Lim, L. Li, Ni doped ZnO thin films for diluted magnetic semiconductor materials, Current Applied Physics 8 (2008) 408–411.
[31] X. Qiu, M. Miyauchi, H. Yu, H. Irie, K. Hashimoto, , Visible-light-driven $Cu(II)-(Sr_{1-y}Na_y)(Ti_{1-x}Mo_x)O_3$ photocatalysts based on conduction band control and surface ion modification, Journal of the American Chemical Society 132 (2010) 15259–15267.
[32] H. Irie, K. Kamiya, T. Shibanuma, S. Miura, D.A. Tryk, T. Yokoyama, K. Hashimoto, Visible light-sensitive Cu(II)-grafted TiO_2 photocatalysts: activities and X-ray absorption fine structure analyses, Journal of Physical Chemistry C 113 (2009) 10761–10766.
[33] Y. Gan, F.B. Gu, D.M. Han, Z.H. Wang, G.S. Guo, Biomimetic synthesis of zinc oxide 3D architectures with gelatin as matrix, Journal of Nanomaterials (2010) 289173–289179.
[34] C. He, T. Sasaki, Y. Shimiz, N. Koshizaki, Synthesis of ZnO nanoparticles using nanosecond pulsed laser ablation in aqueous media and their self-assembly towards spindle-like ZnO aggregates, Applied Surface Science 254 (2008) 2196–2202.
[35] Y.Q. Yang, G.Y. Du, X.L. Ye, Y.S. Zhou, B.D. Xu, A sample method of preparing zinc oxide nanomaterial, New Chemistry Materials 38 (2010) 149–151.
[36] R. Nagaraja, N. Kottam, C.R. Girija, B.M. Nagabhushana, Photocatalytic degradation of rhodamine B dye under UV/solar light using ZnO nanopowder synthesized by solution combustion route, Powder Technology 215 (2011) 91–97.
[37] K. Byrappa, A.K. Subramani, S. Ananda, K.M. Lokanatha Rai, R. Dinesh, M. Yoshimura, Photocatalytic degradation of rhodamine B dye using hydrothermally synthesized ZnO, Bulletin of Materials Science 183 (2010) 315–323.
[38] J.S. Chang, C. Chou, Y.C. Lin, P.J. Lin, J.Y. Ho, L.H. Tai, Kinetic characteristics of bacterial azo-dye decolorization by *Pseudomonas luteola*, Water Research 35 (2001) 2841–2850.
[39] M. Movahedi, A.R. Mahjoub, S. Janitabar-Darzi, Photodegradation of Congo red in aqueous solution on ZnO as an alternative catalyst to TiO_2, Journal of the Iranian Chemical Society 6 (2009) 570–577.
[40] F. Zhang, Y.J. Liu, X.C. Xiao, X.Y. Cai, H. Li, Y.D. Wang, Synthesis and characterisation of highly ordered mesoporous Fe_2O_3–SiO_2 composite and its removal properties of azo dyes from aqueous solution, Materials Technology 27 (2012) 196–206.
[41] J. Yu, J. Ran, Facile preparation and enhanced photocatalytic H_2-production activity of $Cu(OH)_2$ cluster modified TiO_2, Energy and Environmental Science 4 (2011) 1364–1371.
[42] J. Ran, J. Yu, M. Jaroniec, $Ni(OH)_2$ modified CdS nanorods for highly efficient visible-light-driven photocatalytic H_2 generation, Green Chemistry 13 (2011) 2708–2713.
[43] G.K. Pradhan, K.M. Parida, Fabrication of iron–cerium mixed oxide: an efficient photocatalyst for dye degradation, Journal of Engineering Science and Technology 2 (2010) 53–65.